第41卷第11期 无 机 化 学 学 报 Vol.41 No.11
2025年11月 CHINESE JOURNAL OF INORGANIC CHEMISTRY 2371-2384

蜂窝状N、O双掺杂碳/硒复合材料的制备及其碱金属硒电池性能

涂逢樟*,[1] 金钟*,[2]

([1]龙岩学院化学与材料学院,福建省清洁能源重点实验室,龙岩 364012)

([2]南京大学化学化工学院,绿色化学与工程研究院,配位化学全国重点实验室,介观化学教育部重点实验室,清洁能源催化与智能绿色化工江苏省高校重点实验室,苏州市新能源材料与器件绿色智造重点实验室,天长新材料与能源研发中心,南京 210023)

摘要: 设计、制备了一种N、O双掺杂蜂窝状多孔碳(DHPC)作为锂硒(Li-Se)和钠硒(Na-Se)电池的高效硒载体材料。DHPC具有分级多孔结构,可有效封装硒并抑制多硒化物的穿梭效应。结合理论计算证实N、O双掺杂增强了多孔碳对多硒化物的化学吸附作用。Se@DHPC正极在Li-Se电池中表现出高的初始充电容量(675 mAh·g^{-1})和优异的循环稳定性(循环容量衰减率仅0.14%)。在Na-Se电池中也展现出688 mAh·g^{-1}的高容量和300次循环后的高容量保持率。

关键词: 锂硒电池; 钠硒电池; 蜂窝状分级多孔碳; 双杂原子掺杂; 聚硒化物化学吸附

中图分类号: O613.61; O613.52 **文献标识码:** A **文章编号:** 1001-4861(2025)11-2371-14

DOI: 10.11862/CJIC.20250227

Honeycomb-like N, O dual-doped carbon/selenium composites: Preparation and performance in alkali metal-selenium batteries

TU Fengzhang*,[1] JIN Zhong*,[2]

([1]*Fujian Provincial Key Laboratory of Clean Energy Materials, Longyan University, Longyan, Fujian* 364012, *China*)

([2]*State Key Laboratory of Coordination Chemistry, MOE Key Laboratory of Mesoscopic Chemistry, Jiangsu Key Laboratory of Clean Energy Catalysis and Intelligent Green Chemical Engineering, Suzhou Key Laboratory of Green Intelligent Manufacturing of New Energy Materials and Devices, Tianchang New Materials and Energy Technologies Research Center, Institute of Green Chemistry and Engineering, School of Chemistry and Chemical Engineering, Nanjing University, Nanjing* 210023, *China*)

Abstract: A N, O dual-doped honeycomb-like porous carbon (DHPC) was designed and prepared as an efficient selenium host material for lithium-selenium (Li-Se) and sodium-selenium (Na-Se) batteries. The DHPC possessed a hierarchical porous structure that effectively encapsulates Se and suppresses the shuttle effect of polyselenides. Combined with theoretical calculations, it is confirmed that the N, O dual-doping enhances the chemical adsorption of polyselenides. The Se@DHPC cathode delivered a high initial charging capacity of 675 mAh·g^{-1} and excellent cycling stability (with a capacity decay rate of only 0.14% per cycle) in Li-Se batteries. Moreover, it exhibited a high capacity of 688 mAh·g^{-1} and a remarkable capacity retention rate after 300 cycles in Na-Se batteries.

Keywords: Li-Se batteries; Na-Se batteries; honeycomb-like hierarchical porous carbon; dual heteroatom doping; polyselenide chemisorption

收稿日期:2025-07-08。收修改稿日期:2025-10-15。

国家自然科学基金(No.22561160129, 22479074, 22475096)、福建省自然科学基金(No.2021J011094)、博士科研启动基金(No.LB2021010)、装备预研教育部联合基金(No.8091B02052407)、江苏省基础研究计划重点项目(No.BK20253008)、江苏省自然科学基金(BK20240400、BK20241236)、江苏省科技重大专项(No.BG2024013)、江苏省科技成果转化专项资金项目(No.BA2023037)、江苏省学位与研究生教育教学改革课题(No.JGKT24_C001)、苏州市关键核心技术“揭榜挂帅”攻关项目(No.SYG2024122)、苏州实验室开放课题(No.SZLAB-1308-2024-TS005)和郴州国家可持续发展议程创新示范区建设专项(No.2023sfq11)资助。

*通信联系人。E-mail:82001015@lyun.edu.cn,zhongjin@nju.edu.cn

0 Introduction

The rapid development of portable electronic devices and electric vehicles calls for next-generation rechargeable batteries with high energy density, long cycle performance, and low cost. Recently, selenium (Se) cathode materials have attracted increasing attention due to the high theoretical capacity of 3 253 mAh·cm^{-3}, good electronic conductivity of 1×10^{-3} S·m^{-1}, and high density of 4.2 g·cm^{-3}. Due to its numerous advantages, Se cathode material holds great promise for application in alkali metal-Se batteries, including lithium-Se (Li-Se) and sodium-Se (Na-Se) batteries. Nevertheless, due to the shuttle effect of high-order polyselenides, the Se cathode typically exhibits rapid capacity fading and low Coulombic efficiency during cycling[1-3]. To overcome these inherent limitations, infiltrating Se into carbon matrix materials, such as porous carbon[4-6], metal-organic framework-derived composites[7-9], carbon nanofibers/nanotubes[10], and graphene[11], would be beneficial. Although such Se/C hybrids enhance the conductivity and exhibit good electrochemical properties in the initial stage, the long cycle performance is usually poor due to the following three reasons: (a) weak interaction between Se and carbon host; (b) volume expansion during the cycle; (c) side reactions between Se anions and electrolytes[12]. Therefore, it is of great importance to design novel Se composite cathodes to enhance the chemical binding and overcome the inherent limitations, thus improving the cycle life and Coulombic efficiency of Li-Se and Na-Se batteries[11]. It is expected that the heteroatom (N, O, P, and so on) doping of nanocarbon materials can essentially enhance the binding force between Se species and carbon hosts for dramatically improving the electrochemical performances.

Herein, we report the design and construction of a hybrid Se composite cathode (Se@DHPC), which involves loading amorphous Se onto a honeycomb porous carbon matrix dual-doped with N and O heteroatoms (DHPC). The DHPC support was synthesized via a novel microwave puffing technique—an atmospheric pressure puffing process that utilizes radiation heat transfer to enable uniform and rapid heating of the precursor. This method effectively overcomes the instability issues associated with conventional hot air drying caused by non-uniform expansion. Although microwave puffing has been widely adopted in food processing, its application in the preparation of carbon nanomaterials remains scarcely explored. In this work, popcorn, a maize variety specifically designed for microwave popping due to its excellent puffing characteristics[13], was employed as the carbon source. Se@DHPC had a high density, a large specific surface area, a large pore volume, and a unique nano-architecture composed of connected macro/meso/micropores. The unique structure of Se@DHPC had three crucial characteristics: (a) the carbon matrix provides superior electronic conductivity; (b) the hierarchical nanopore structure provides abundant electrolyte channels while acting as a microreactor, which effectively inhibits the electrode volume expansion and captures the polyselenide intermediates in the redox reaction process; (c) the dual-doping of N and O boosts the chemical absorption and interaction of the carbon matrix with Se and Li_2Se_x/Na_2Se_x species. Hence, the synergistic effect of heteroatom (N and O) dual-doping and vesicular nanoporous structure significantly enhances the cycle performance and rate capability of alkali metal-Se batteries[14]. As a result, the Li-Se and Na-Se batteries based on Se@DHPC composite cathodes delivered high rate capability and excellent cycle stability. For Li-Se batteries, the initial specific capacity of Se@DHPC cathode was 675 mAh·g^{-1} at the current density of 0.2C (1C=678 mA·g^{-1}), with a nearly 100% Coulombic efficiency and a capacity decay rate as low as 0.14%. For rechargeable Na-Se batteries, the Se@DHPC composite cathode exhibited an initial specific capacity of 688 mAh·g^{-1} at 1C, and the specific discharge capacity was still maintained at a high level after 300 cycles.

1 Experimental

1.1 Synthesis of DHPC

All chemicals and reagents were of analytical grade and used without further purification. Hydrochloric acid (HCl) and potassium hydroxide (KOH) were purchased from Sinopharm Chemical Reagent Co., Ltd.

The nubby maize grains were obtained from a Taobao Online Store. Firstly, the nubby maize was extruded by a 700 W microwave for 2 min to turn into popcorn. Subsequently, after continued microwave treatment for 10 min, popcorn charcoal flakes (PCF) were prepared with a yield of about 53%. Then, PCF and KOH (1∶3, *w*/*w*) were ground and mixed evenly, and heated to 650 ℃ at a rate of 5 ℃ min^{-1} in Ar gas protection, and then activated for 2 h. Black solids were washed successively with 1 mol·L^{-1} HCl and 10% HF solution, and then thoroughly washed with deionized water and ethanol to obtain the DHPC matrix. The weight loss of the DHPC sample was about 68.2%. Finally, the samples were dried at 100 ℃ for 12 h under a vacuum drying procedure.

1.2 Synthesis of Se@DHPC

Se@DHPC was prepared by a simple melt diffusion method. The pure Se and DHPC were mixed and ground evenly in an agate mortar with a weight ratio of 6∶4. After desiccation, the mixture was transferred to a quartz tube furnace. Se@DHPC was obtained by keeping it at 260 ℃ for 8 h in an Ar atmosphere.

1.3 Characterizations

X-ray powder diffraction (XRD) measurements were performed on a Rigaku Smartlab diffractometer with Cu *Kα* radiation (λ=0.154 06 nm) at 40 kV and 40 mA, over a 2θ range of 5° to 80° at a scanning rate of 5 °·min^{-1}. The morphology features were characterized by a JEOL JSM-7600F field-emission scanning electron microscopy (SEM). Using transmission electron microscopy (TEM, JEOL JEM-2100F, 200 kV) and energy dispersive X-ray spectroscopy (EDX, ESCALab 250xi electron spectrometer), the microstructures and spatial element distributions were obtained. Thermogravimetric analysis (TGA) was carried out in N_2 atmosphere with NETZSCH STA 449 F3 thermogravimetric analyzer from room temperature to 800 ℃ at the heating rate of 10 ℃·min^{-1}. Raman spectra were measured by a LabRAM HR Raman spectrometer with a 523 nm diode solid state laser and a Nd line laser source. X-ray photoelectron spectroscopy (XPS) was performed on an ESCALAB spectrometer using a Mg *Kα* light source. FTIR spectra were performed on a Bruker Tensor IFS-66V/S spectrometer. Specific surface areas and pore size distributions of the samples were analyzed by the ASAP 2020 specific surface area and pore size tester. The pore size distribution was calculated by the Barrett-Joyner-Halenda (BJH) method and Horvanth-Kawazoe (HK) method.

1.4 Electrochemical tests

The electrochemical performances of the Se@DHPC cathode were tested by CR-2032 coin cells assembled in a glove box filled with high-purity argon. Se@DHPC, Super P carbon black, and polyvinylidene fluoride adhesives were ground and mixed evenly with a weight ratio of 8∶1∶1. The obtained slurry was evenly coated on an aluminium foil and vacuum-dried for 12 h at 80 ℃. The load of active materials was about 1.5 mg·cm^{-2}, and the foil was cut into a round disk of 10 mm diameter. The Li-Se coin cells were assembled with Li foil as the counter electrode, and the electrolyte was 1.0 mol·L^{-1} $LiPF_6$ ethylene carbonate (EC)/diethyl carbonate (DEC) (1∶1 in volume). The electrolyte dosage of each battery was 200 μL, and the separator was Celgard 2400 membrane. The assembly conditions for the Li-Se soft-package batteries followed a similar procedure, wherein the cells were encapsulated using an aluminum-plastic composite film and vacuum-sealed to ensure mechanical integrity and prevent electrolyte leakage. Similarly, the sodium foil was used as the counter electrode for the Na-Se battery, and 1.0 mol·L^{-1} sodium perchlorate ($NaClO_4$) in a mixture of EC and DEC (1∶1 in volume) was used as the electrolyte, and the amount of electrolyte used in each cell was 200 μL. Whatman glass fiber membrane was used as the separator for Na-Se batteries. The constant current charge/discharge performances were tested on a LAND-2100 battery testing instrument (Wuhan, China) at room temperature, and the specific capacity was calculated based on the loading mass of Se. The cyclic voltammetry (CV) curves of electrode materials were carried out on a VersaSTAT 4 electrochemical workstation in the voltage ranges of 1.0-3.0 V (vs Li/Li^+) for Li-Se batteries, and 0.8-3.0 V (vs Na/Na^+) for Na-Se batteries.

1.5 Calculation

To better understand the superior electrochemical

performances of Se@DHPC as cathodes for Li-Se and Na-Se batteries, density functional theory (DFT) calculations were performed to model the adsorption between Li_2Se and Na_2Se with various doped and undoped carbon substrates. The optimization of all the structures was as per the Vienna Ab Simulation Package (VASP), where the Perdew-Burke-Ernzerhof (PBE) functional of the generalized gradient approximation (GGA) described the exchange-correlation potential. During the calculations, the cutoff energy was at 400 eV, and the convergence criteria of electron energy and residual force were 10^{-4} eV and 0.5 eV·nm^{-1}, respectively. The Γ-centered 4×1×1 k-points mesh was sampled in the Brillouin zone. The 1.5 nm vacuum layer decreased the interlayer interaction.

2 Results and discussion

2.1 Morphology and composition of the electrodes

Fig. 1a illustrates the synthesis process of DHPC and Se@DHPC. Firstly, the heated endosperm of corn generated steam and increased the pressure. With the pressure exceeding the bearing capacity of the peel, the seeds burst and expand to produce nutritious, crisp, and delicious popcorn. For this variety, the popping rate was generally 80%-98%, and the expansion ratio was 9-30 times. Instantaneously, a unique honeycomb-like flake structure formed during the expansion process (Fig. 1a). Through the expansion effect of the microwave pulse, hierarchical porous structures were prepared from granular biomass materials. The microwave expansion effect showed numerous advantageous characteristics, including high energy conversion efficiency, fast heating speed, no heat radiation waste, no powder sound, no noise, no pollution, and so on. Subsequently, the DHPC material was prepared from the popcorn after thermal carbonization and alkali activation. Finally, Se@DHPC was obtained via Se loading, which can serve as a high-performance cathode material in alkali metal-Se batteries.

Fig. 1b demonstrates the XRD patterns of pure Se, DHPC, and Se@DHPC. All the diffraction peaks obtained for pure Se could be well-matched with the crystalline trigonal Se, indicating high thermal stability for Se. After the melting-diffusion process, all the diffraction peaks of Se disappeared in Se@DHPC, suggesting that the amorphous Se had good dispersibility in the DHPC pores. The results of Raman analyses were in good agreement with the XRD patterns, as exhibited in Fig. 1c[15]. Raman analysis confirms the transition from crystalline trigonal Se (peak at *ca*. 235 cm^{-1}) in pure Se to amorphous cyclic Se_8 molecules (peaks at *ca*. 113 and *ca*. 250 cm^{-1}) within the Se@DHPC composite. This amorphous state promotes better dispersion and contact with the carbon matrix, improving reaction kinetics. The two peaks at 1 603 and 1 345 cm^{-1} in the Raman spectra of DHPC and Se@DHPC represent crystalline graphite (G band) and disordered graphite (D band), respectively[16]. Simultaneously, the results of Raman spectra revealed that the carbon layer of Se@DHPC had a lower intensity ratio (I_D/I_G) of D band to G band after Se loading, indicating a higher graphitization degree, and a more compact and regular carbon layer structure[17]. It is due to the elongation of the sp^2 carbon skeleton of DHPC, which terminates the dangling carbon bond after loading Se molecules[18].

The specific surface area, micropore volume, and total pore volume of DHPC calculated by the BET (Brunauer-Emmett-Teller) method were 1 234 m^2·g^{-1}, 0.521 1 cm^3·g^{-1}, and 3.391 1 cm^3·g^{-1}, respectively. The pore-size distribution curve of DHPC revealed the predominant position of the micropore at 0.30 nm (Fig. 1d, 1e), and a small number of mesopores with a size of 30-40 nm. After Se loading, the micropore disappeared, and the mesopore decreased significantly in Se@DHPC. The pore volume and specific surface area of Se@DHPC decreased to 0.002 1 cm^3·g^{-1} and 4 m^2·g^{-1}, respectively, which demonstrates the effective loading of Se into the composite pores of DHPC. Notably, the abundant micropores can effectively confine the polyselenides in DHPC and boost the movement of Li^+ and electrons that allow a large amount of active substance Se to participate in electrochemical reactions, thereby effectively alleviating the shuttle effect of the polyselenides[19]. According to the micropore volume calcula-

tion, the upper limit of Se loading amount (mass fraction) in DHPC was approximately 60%. Noticeably, after Se impregnation, some unoccupied voids in the micropore can effectively counter the volumetric expansion of active substances in the circulation process, hence avoiding structural breakdown and restraining side reactions. Therefore, the appropriate amount of loaded Se is imperative for the best electrochemical performance, as further confirmed by electrochemical tests. The TGA shown in Fig. S1 (Supporting information) revealed that the mass fraction of Se encapsulated within Se@DHPC was approximately 53.0%. Se@DHPC had a higher Se gasification temperature than pure Se, indicating stronger interactions between Se and DHPC. It can be further proved by infrared spectroscopy and other means, which are conducive to improving cycling performance and rate characteristics of Se@DHPC. Interestingly, the weight loss process of Se@DHPC consists of two gasification processes, *i.e.*, attribution of the low-temperature section to the vaporization of excessive Se adhering to the outer surface of the DHPC matrix and attribution of the high-temperature segment to the vaporization of Se in the DHPC inner-pores[20].

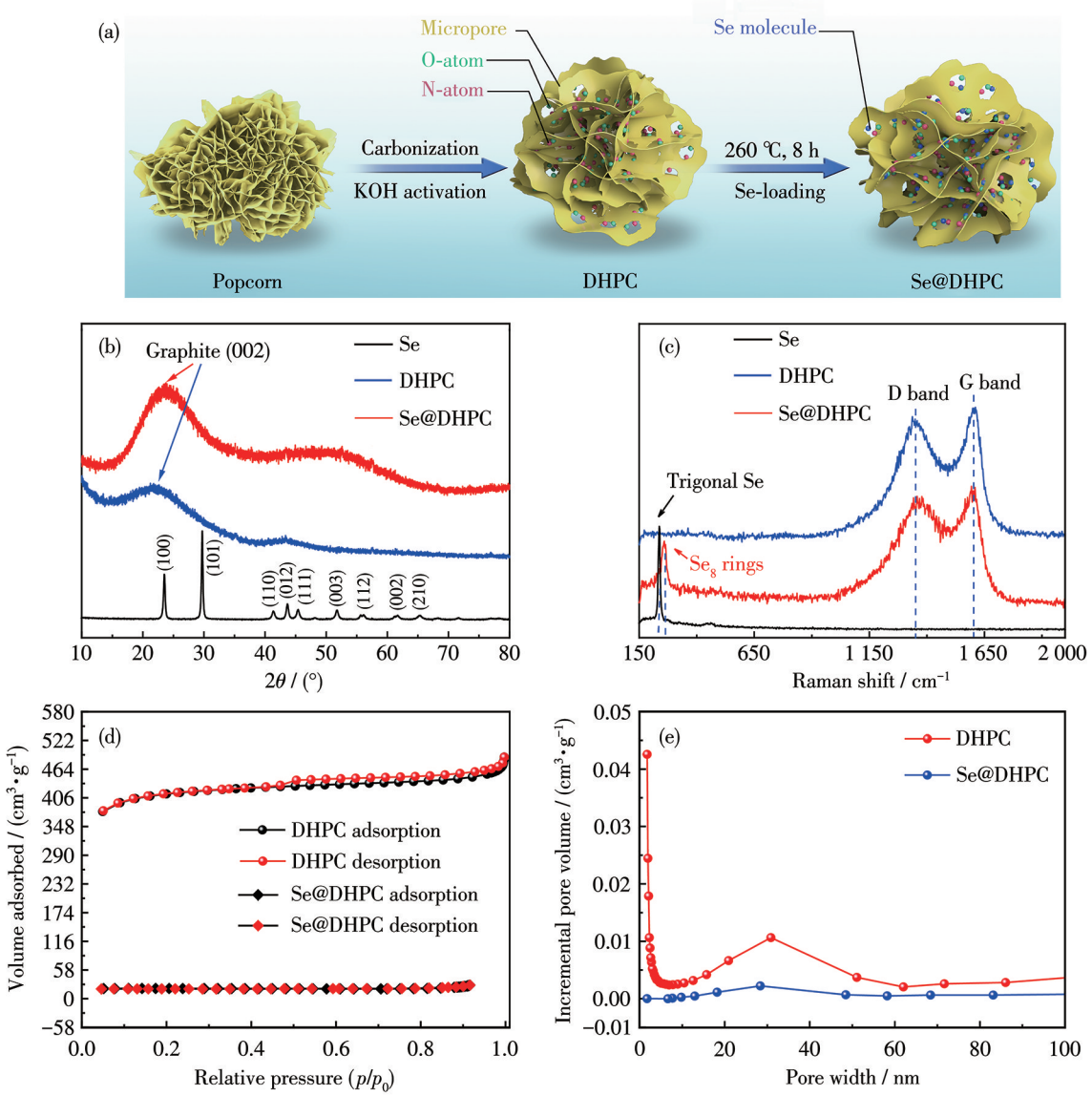

Fig. 1　(a) Synthesis process schematic of Se@DHPC; (b) XRD patterns and (c) Raman spectra of pure Se, DHPC, and Se@DHPC; (d) N_2 adsorption-desorption isotherms of DHPC and Se@DHPC at 77 K; (e) Pore-size distribution curves of DHPC and Se@DHPC calculated via the BJH method

The SEM images in Fig.2a and 2b depict the three-dimensional honeycomb-like structure of DHPC with an interconnected porous structure. The TEM (Fig.2c) analysis of DHPC revealed a hierarchical porous surface and structure. As illustrated in Fig.2d and 2e, the porous features and microstructure could be well-maintained after Se loading, and no noticeable Se particles or powders could be observed on the exterior surface of Se@DHPC. High-resolution transmission electron microscopy (HRTEM) image (Fig.2f) showed only the highly disordered sp^2 carbon lattice fringes of DHPC, demonstrating the amorphous nature of the Se loaded in Se@DHPC[21-23]. The above results showed the successful encapsulation of the majority of the Se into the inner pore of the DHPC matrix. Furthermore, the elemental distribution revealed the uniform spatial distribution of Se, N, C, and O elements in Se@DHPC, as shown in Fig.2g-2k.

XPS analysis further reveals the chemical states of the elements of Se@DHPC (Fig.3a-3d, S2). In the C1*s* XPS high-resolution spectrum (Fig.3a), the peaks at 284.8 eV indicate the sp^2-hybridized carbon with C—C configuration. The peaks at 285.7, 286.8, and 289.3 eV are ascribed to the C—O, C—N, and C=O species, respectively, which distinctly corroborate the successful embedding of heteroatoms (O and N) in the honeycomb-like carbon matrix. The XPS spectra of the N and O elements (Fig.3b and 3c) reveal the abundance of N-, O-functional groups in DHPC[24-26], with the N and O contents (atomic fractions) of 4.28% and 11.66%, respectively. Fig.3c shows the N1*s* spectrum, which consists of pyrrolic N (400.9 eV), graphitic N (402.6 eV), and oxidized N (399.8 eV). The O1*s* XPS spectrum in Fig.3c indicates the presence of O species as C=O (532.1 eV), C—O (532.8 eV), hydroxyl O (533.9 eV), adsorbed O (535.1 eV), and carboxylic O

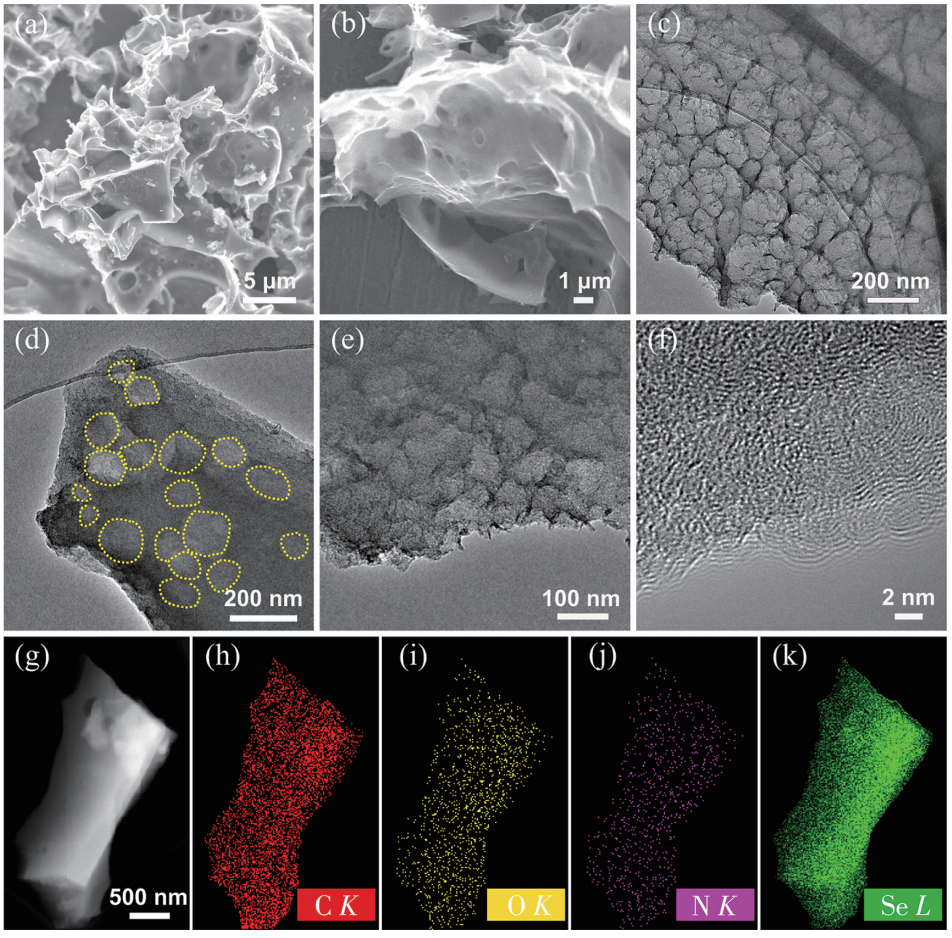

Fig.2 (a, b) SEM and (c) TEM images of DHPC; (d, e) TEM and (f) HRTEM images of Se@DHPC; (g-k) Elemental distribution mappings of Se@DHPC

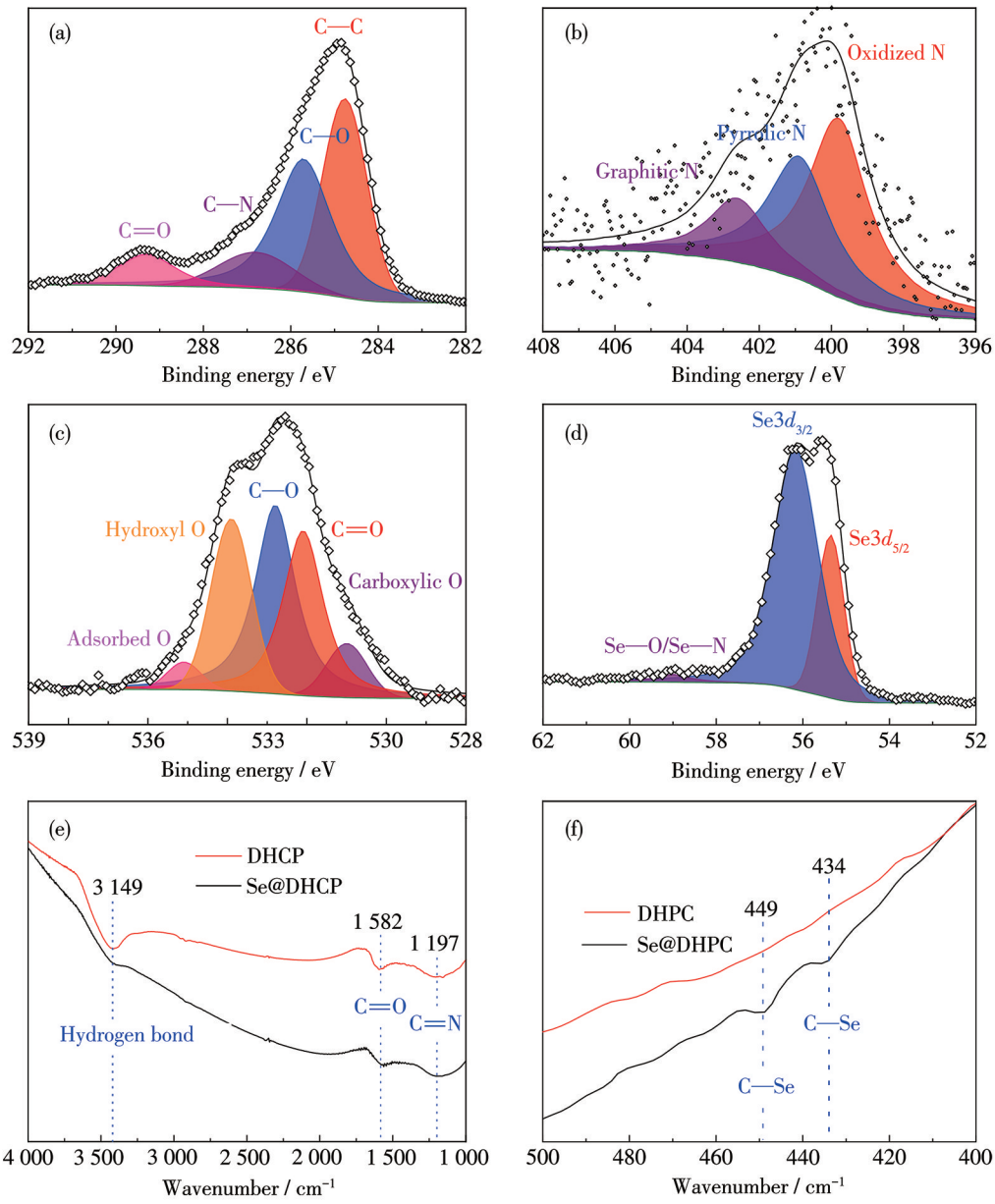

Fig.3　(a) C1*s*, (b) N1*s*, (c) O1*s*, and (d) Se3*d* XPS spectra of Se@DHPC; (e, f) FTIR spectra of DHPC and Se@DHPC

(531.0 eV). The Se3*d* XPS spectra (Fig.3d) showed the binding energies centered at 55.4 and 56.2 eV, respectively, corresponding to Se3$d_{5/2}$ and Se3$d_{3/2}$ due to the spin-orbit coupling[27]. These binding energies are characteristic of metallic Se^0, confirming the predominant presence of metallic Se^0 in Se@DHPC. The peak centered at 59.0 eV can be attributed to Se—O and Se—N bonds, which reveals a strong interaction between N and O dual-doped carbon and Se-containing species conducive for the electrochemical stability in Li-Se batteries[27-28]. Furthermore, FTIR spectra measured the bonding interactions of DHPC and Se@DHPC. As illustrated in Fig. 3e and 3f, the FTIR spectra of the two samples indicate the fine signature signals of the hydrogen bond at 3 149 cm^{-1}, the C=O bond at 1 582 cm^{-1}, and the C=N bond at 1 197 cm^{-1}. The two new peaks at 449 and 434 cm^{-1} can be attributed to the bending vibration of C—Se bond, which reveals a significant chemical affinity between Se and DHPC matrix[28].

2.2　Electrochemical behavior

To study the cyclic performance and rate characteristics of Se@DHPC in alkali metal-Se batteries, a Li or Na foil was used as the counter electrode to assemble the coin cells in carbonate-based electrolytes. The

Li-Se batteries based on Se@DHPC cathode were preliminarily investigated by CV curves (Fig. 4a). During the lithiation/delithiation processes, Se@DHPC had only one pair of reversible redox peaks, demonstrating a single-phase change electrochemical reaction between Se-containing species in 1 mol·L^{-1} $LiPF_6$ with EC/DEC (1∶1, *V*∶*V*)[29]. The activation process detected during the initial discharge step may be related to the Se@DHPC composite deformation caused by the volume change[18,30]. The significant overlap of CV curves after the second loop indicated the high redox reversibility and good cycle stability of Se@DHPC[27,31-32].

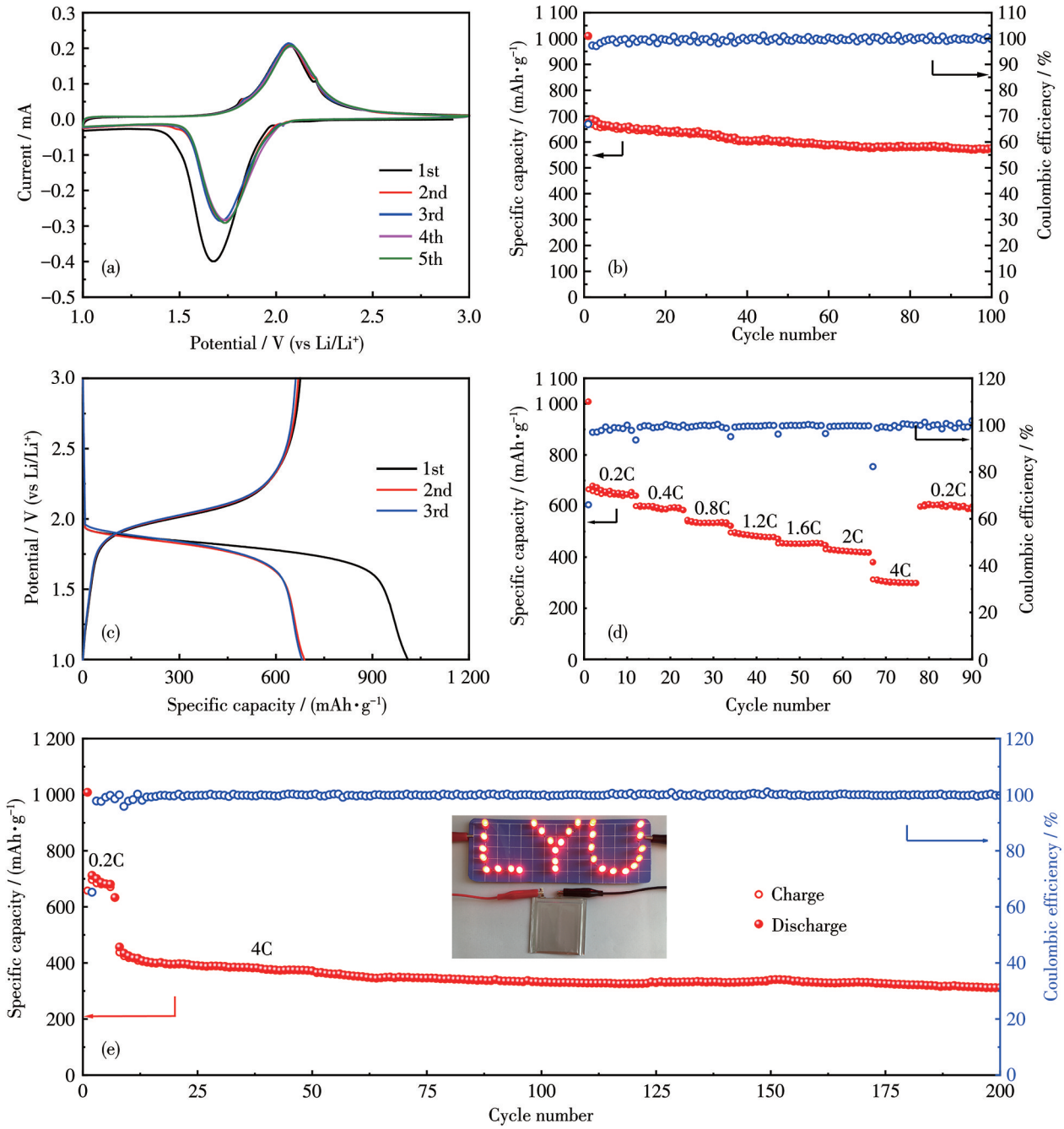

Inset: the photographs of LED lamps with the pattern of "LYU" lighted by Se@DHPC based soft-packed Li-Se batteries.

Fig.4 Li-Se battery performance based on Se@DHPC cathode: (a) CV curves at a sweep rate of 0.1 mV·s^{-1}; (b) cycling performance at 0.2C; (c) galvanostatic discharge/charge curves for the 1st, 2nd, and 3rd cycles at 0.2C; (d) rate performance under various current densities; (e) long cycling performance at 4C

Fig. 4b presents the cycling performance of the Se@DHPC cathode in Li-Se batteries at 0.2C. At the initial cycle, the high irreversible specific capacity loss (Fig.4b) was usually met with the irreversible reactions between Li and surface functional groups and the formation of a solid electrolyte interface (SEI) layer by the electrolyte[33]. Besides, Se@DHPC could achieve high initial reversible specific capacities of 675 mAh·g^{-1}. After the first few cycles, Se@DHPC showed a high reversible specific capacity of 578 mAh·g^{-1} with 84% capacity retention rate after 100 cycles. Thus, the excellent capacity retention of Se@DHPC confirms the cooperative effect of diatomic doping in the porous carbon matrix. The electrochemical characteristics of Se@DHPC are demonstrated in Fig.4c by galvanostatic discharge/charge evaluation in the voltage range of 1.0-3.0 V at 0.2C (135.6 mA·g^{-1}). The cathode exhibited a ramp voltage platform similar to the CV curve, which further verifies and validates the existence of only a single-phase change electrochemical reaction in the charging/discharging process. As shown in Fig.4c, the initial specific discharge and charge capacities of Se@DHPC were 1 010 and 676 mAh·g^{-1}, respectively. Due to the irreversible formation of the SEI layer, the irreversible capacity of the first cycle was 334 mAh·g^{-1} [34-35]. Notably, the gaps between lithiation and delithiation profiles did not significantly alter with the deepening of the cycle, which confirms good electrochemical stability of Se@DHPC composite[32,36]. The as-prepared Se@ DHPC composite exhibited excellent rate performance, as shown in Fig.4d. Se@DHPC provided a high reversible specific capacity of 315 mAh·g^{-1} even at a high current density of 4C (2.72 A·g^{-1}). With the current density returning to 0.2C, the discharge specific capacity reverted to 608 mAh·g^{-1}. Fig. 4e depicts the excellent cycling stability of Se@DHPC in lithium storage. After 200 cycles, the composite provided a stable, reversible specific capacity of 312 mAh·g^{-1} at 4C with nearly 100% Coulombic efficiency, revealing high rate performance and good cyclic stability. Simultaneously, it showed a very low specific capacity decay rate of only 0.14% per cycle. To demonstrate the practical potential of using visual identification, Se@DHPC based soft-packed Li-Se batteries were assembled, which can easily power a series of light-emitting diodes (LEDs) with "LYU" pattern, as displayed in the insets of Fig.4e. Compared to Se@DHPC, Fig.S3 demonstrates much inferior electrochemical properties of pure Se and DHPC electrodes. The first reversible discharge specific capacity for DHPC was 91.6 mAh·g^{-1}. After 100 cycles, the reversible specific capacity was only 17.3 mAh·g^{-1}, revealing the negligible capacity contribution from DHPC in Se@DHPC. Compared to the original electrode (Fig.S4a, S4b), the SEM image of the Se@DHPC electrode after cycling (Fig.S4c, S4d) revealed that the morphology remained substantially unchanged after the cycling, indicating the good structural stability of Se@DHPC. Thus, all the above results showed that the prepared Se-loaded DHPC cathode material had superior electrochemical stability and rate characteristics.

To further study the strong interaction between the DHPC matrix and Se species, Se@DHPC was further investigated after 200 cycles. It revealed that the battery separator assembled with Se@DHPC had no significant color change (Fig. S5), which revealed the sufficiently confined Se species within the pores of the DHPC matrix during charging and discharging. Fig.S6 depicts the Nyquist plots of pure Se and Se@DHPC in Li-Se batteries, confirming the outstanding electrochemical performance of Se@DHPC. According to previous literature[29], among various heteroatom-doped carbons, N and O dual-doped carbon had the best binding effect on Li_2Se, which is significant evidence of a strong interaction between Se/selenides and DHPC matrix. In this paper, the moderate calcination temperature provides higher contents of pyrrolic N and ketone-O species in DHPC, which efficiently improves the electrochemical performance of Se-loaded DHPC composite for alkali metal-Se batteries.

As discussed above, the Se@DHPC hybrid material had excellent properties for lithium storage. Considering the electrochemical similarity between lithium and sodium storage, we further investigated the energy storage characteristics of Se@DHPC as a cathode electrode for Na-Se batteries. As expected, Se@DHPC also

exhibited good electrochemical properties in Na-Se batteries containing 1 mol·L^{-1} $NaClO_4$ with the EC/DEC electrolyte. We first investigated the CV characteristics of Se@DHPC during sodium storage, as shown in Fig.5a. The cathodic peaks at 1.11 V and anodic peaks at 1.75 V in the first cycle are attributed to the redox reaction of Se and Na^+ ions, which moved to a higher voltage and remained stable subsequently. From the second cycle, the shift of the cathodic peak to 1.20 V indicates the formation of Na_2Se_2[24]. Next, we investigated the galvanostatic cycling performance of Se@DHPC in Na-Se batteries, as shown in Fig.5b. Encouragingly, the initial discharging and charging capacities were 1 058 and 723 mAh·g^{-1}, respectively. The Coulombic efficiency of the first cycle was nearly 58%. The capacity loss is due to the irreversible capacity of the DHPC matrix and the formation of the SEI film. The cycling performance of Se@DHPC for sodium storage was slightly worse than that of lithium storage, which is essentially due to the poor kinetics of the electrochemical reaction attributed to the larger radius of Na^+ and the volume expansion. As shown in Fig.5c, the reversible specific capacity of Se@DHPC in Na-Se batteries after 100 cycles at 0.2C was 404 mAh·g^{-1}, corresponding to a specific capacity retention rate of 59.0%, verifying the relatively stable electrochemical performance of Se@DHPC. In contrast, the pure Se and DHPC electrodes showed a relatively inferior electrochemical performance, as shown in Fig.S7a and S7b. Fig.5d shows the long cycling characteristics of the Se@DHPC cathode. In the initial three cycles, the electrode provided a reversible capacity of 688 mAh·g^{-1} at 0.2C. Even at a high current density of 1C, a high discharge specific capacity of 343 mAh·g^{-1} could be maintained after 300 cycles. Notably, the glass fiber separator in the Na-Se battery assembled with Se@DHPC cathode showed a much lighter color than that with a pure Se electrode, as depicted in the insets of Fig.5d, indicating the sufficient inhibition of polyselenide shutting by the DHPC matrix. Furthermore, the honeycomb-like morphology of Se@DHPC did not change after 100 cycles at 0.1C (Fig. S8a, S8b), because the DHPC matrix effectively buffered the volume change.

To further reveal the high-rate characteristics of the Se@DHPC cathode for Na storage, the tests of CV curves at different scanning rates are depicted in Fig.6a. The relationship between the peak current (i_p) and the scan rate (v) is $i_p=av^b$, where a and b are variables[37]. The slope of lg i_p vs lg v provides the value of b. Notably, the calculated b values for all reduction and

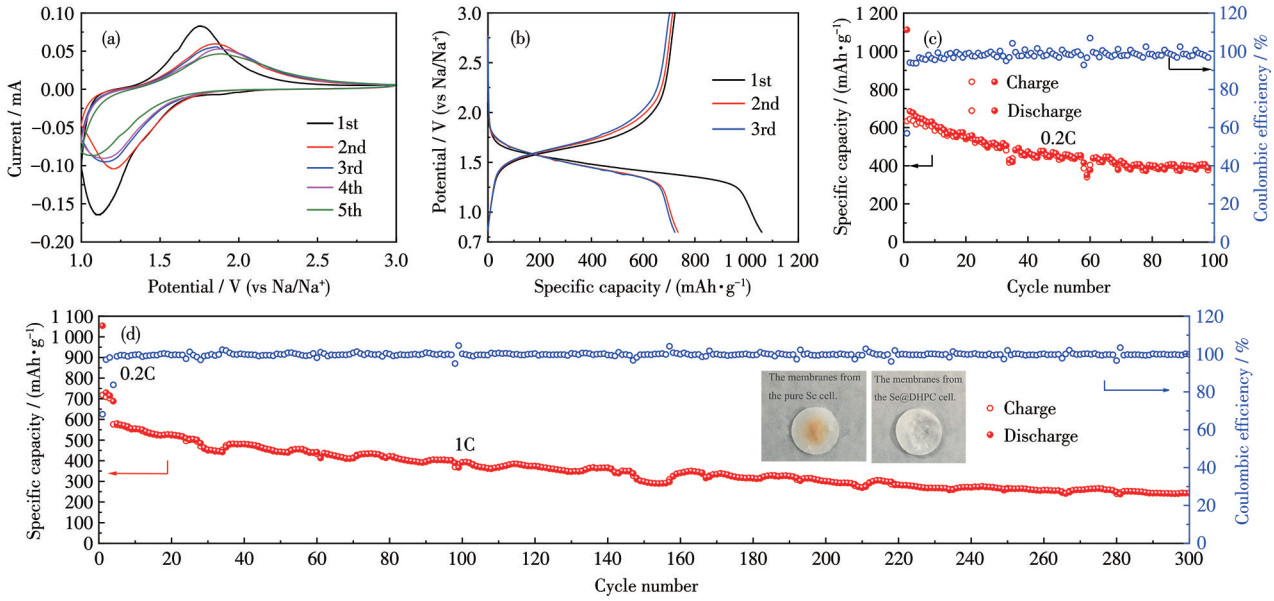

Inset: the digital photos of the separator membranes with the pure Se and Se@DHPC cathodes after 100 cycles, respectively.

Fig.5 Na-Se battery performance of Se@DHPC: (a) CV curves at a sweep rate of 0.1 mV·s^{-1}; (b) galvanostatic discharge/charge curves for the 1st, 2nd, and 3rd cycles at 0.2C; (c) cycling performance at 0.2C; (d) long cycling performance at 1C

oxidation peaks were higher than 0.55, indicating capacitance-induced capacity as the main contributor to the cycling processes (Fig.6b). To further elucidate the contribution ratio of diffusion- and capacitive-dominated processes, the current (i_V) at a specific potential (V) can be expressed as the sum of capacitive effect (k_1v) and diffusion-dominated reaction ($k_2v^{1/2}$), calculated as $i_V=k_1v+k_2v^{1/2}$. The constants k_1 and k_2 can distinguish the contribution of surface capacitance and diffusion. The typical voltage curve (Fig.6c) showed that the capacitive contribution (the blue part) dominated the total specific capacity. With increasing the scanning rate, the capacitive contribution of Se@DHPC in Li-Se batteries gradually increased, showing a value of

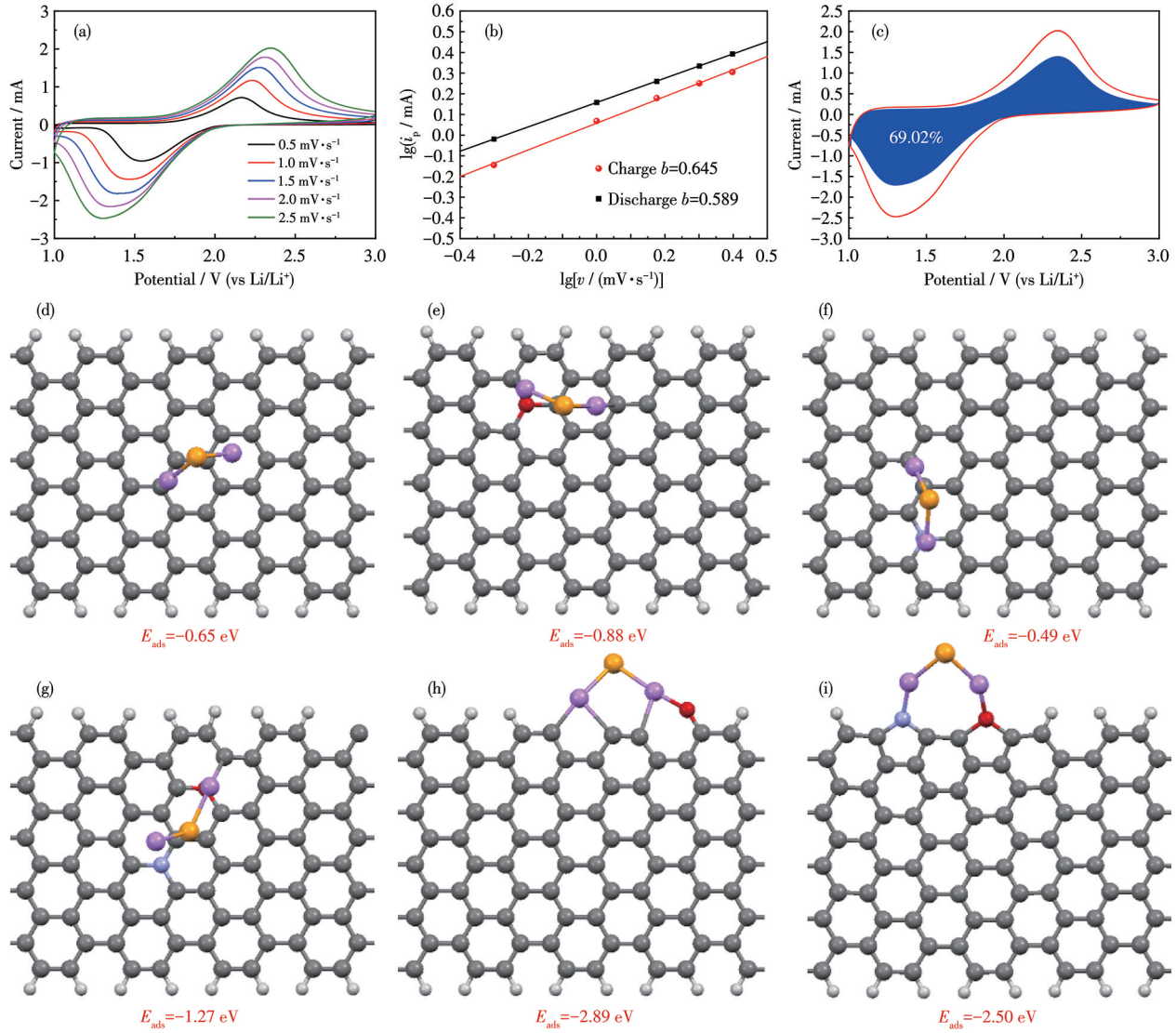

The gray, white, red, blue, purple, and brown balls represent C, H, O, N, Se, and Na atoms, respectively; (d) Undoped carbon substrate, adsorption site: Na_2Se physically adsorbed on the sp^2-carbon plane; (e) O-doped carbon substrate (ketonic O), adsorption site: Na coordinated with ketonic O atom; (f) N-doped carbon substrate (pyrrolic N), adsorption site: Na coordinated with pyrrolic N atom; (g) N, O-co-doped carbon substrate (pyrrolic N+ketonic O), adsorption site: Na simultaneously coordinated to N and O atoms; (h) O-doped zigzag edge, adsorption site: Na bonded with carboxylic O at the edge; (i) N, O-co-doped zigzag edge, adsorption site: Na dual-coordinated with pyrrolic N and carbonyl O at the edge.

Fig.6　Quantitative kinetics analysis of Se@DHPC for Li-Se batteries and DFT calculation for Na-Se batteries: (a) CV curves at different scan rates; (b) determination of the b-value by the relationship between the scan rate and the peak current; (c) capacitive contribution (the blue section) at 2.5 mV·s^{-1}; (d-i) DTF simulation optimized chemisorption structure of Na_2Se on doped and undoped carbon substrates

69.02% at 2.5 $mV \cdot s^{-1}$ (Fig.S9). The quantitative kinetics analysis revealed the surface capacitive reaction as the dominant process, which is the reason for the high rate capability of Se@DHPC.

To better understand the superior electrochemical performances of Se@DHPC as cathodes for Li-Se and Na-Se batteries, DFT calculations were performed in Fig.S10a-S10f and Fig.6d-6i. The DFT-D3 method was also considered to depict the adsorption behavior of Na_2Se on the carbon substrate. The definition of adsorption energy (E_{ads}) was as follows:

$$E_{ads}=E_{total}-E_{slab}-E_m \quad (1)$$

Here, the adsorption energy was computed as the difference between the energy of the adsorption complex (E_{total}), the energy of the clean carbon substrate (E_{slab}), and the energy of the free Se-containing molecule Li_2Se or Na_2Se (E_m). The DFT calculations predicted the adsorption behavior of Li_2Se and Na_2Se on carbon substrates doped with N (N—C), O (O—C), and N and O (N—C/O—C). To assess the chemisorption of Na_2Se in the nanopores of the DHPC cathode for Na-Se batteries, Fig.6d-6i show the optimized adsorption model and corresponding E_{ads} between N and/or O-doped carbon and Na_2Se. As revealed by the simulation results, the binding energy of Na_2Se on the surface of doped carbon was −0.76 eV on N—C (Fig.6f), −0.77 eV on O—C (Fig.6e), and −1.23 eV on N—C/O—C (Fig.6g), respectively, which are lower than that of undoped carbon (−0.28 eV, Fig.6d). It verifies that both N and O doping can enhance the adsorption of Na_2Se on the surface of carbon substrate. Thus, the Na_2Se binds strongly on the N and O dual-doped carbon, showing a more negative adsorption energy of −1.23 eV than solely N- or O-doped carbon (*ca.* 0.76 eV). Besides, the zigzag edge doped by O (Fig.6h) or N, O (Fig.6i) enables stronger Na_2Se binding with the binding energy of −2.61 and −2.09 eV, respectively, due to the electron unsaturation of edge-doped N and O species. For Li-Se batteries, similar conclusions can also be obtained (Fig.S10). These results prove that the pyrrolic-N and ketone-O species in the DHPC matrix provide strong binding and chemisorption of Li_2Se and Na_2Se, leading to excellent electrochemical energy storage characteristics for lithium and sodium storage.

3 Conclusions

This paper presents a well-designed cathode material with Se confined in a heteroatom (N and O) dual-doped porous carbon matrix for alkali metal-Se batteries. The as-prepared Se@DHPC composite showed excellent cycling performance and rate characteristics for lithium and sodium storage. The material characterizations, battery tests and DFT analyses evidence the outstanding electrochemical properties of Se@DHPC cathode, which can be summarized as: (1) the hierarchical macro/meso/micropores with interconnected channels provides a fast transport pathway for Li^+/Na^+ ions during charging and discharging, and thus enhancing the rate capability and specific capacity retention; (2) the micropores in DHPC are conducive to Se loading and have a spatial limitation effect on Se species, which alleviates the volume expansion during long cycling; (3) short-chain Se molecule in micropore are easily formed, which can reduce side reactions; (4) the dual-doping of N and O heteroatoms can adjust the electronic structure and effectively improving the interactions with Se species with carbon matrix. The rational design and construction of high-performance Se@DHPC cathode material show great potential for applications in next-generation alkali metal-Se battery systems.

Acknowledgements: This work was supported by the National Natural Science Foundation of China (Grants No. 22561160129, 22479074, 22475096), the Natural Science Foundation of Fujian Province (Grant No. 2021J011094), the Doctoral Research Initiation Fund (Grant No. LB2021010), the Equipment Pre-research and Ministry of Education Joint Fund (Grant No. 8091B02052407), the Fundamental Research Program Key Project of Jiangsu Province (Grant No. BK20253008), the Natural Science Foundation of Jiangsu Province (Grants No. BK20240400, BK20241236), the Science and Technology Major Project of Jiangsu Province (Grant No.BG2024013), the Scientific and Techno-logical Achievements Transformation Special Fund of Jiangsu Province (Grant No.BA2023037), the Academic Degree and Postgraduate Education Reforming Project of Jiangsu Province (Grant No.JGKT24_C001), the Key Core Tech-

nology Open Competition Project of Suzhou City (Grant No. SYG2024122), the Open Research Fund of Suzhou Laboratory (Grant No.SZLAB-1308-2024-TS005), and the Chenzhou National Sustainable Development Agenda Innovation Demonstration Zone Provincial Special Project (Grant No.2023sfq11).

Supporting information is available at http://www.wjhxxb.cn

Author contributions: Tu Fengzhang conceived the idea of this manuscript, Tu Fengzhang prepared, characterized, and tested the samples, Tu Fengzhang and Jin Zhong analyzed the results, and co-wrote the paper.

Conflict of interest: The authors declare no conflicts of interest.

References:

[1]ZHANG F, GUO X, XIONG P, ZHANG J Q, SONG J J, YAN K, GAO X C, LIU H, WANG G X. Interface engineering of MXene composite separator for high-performance Li-Se and Na-Se batteries[J]. Adv. Energy Mater., 2020,10(20):202000446

[2]QI X Q, YANG Y, JIN Q, YANG F Y, XIE Y, SANG P F, LIU K, ZHAO W B, XU X B, FU Y Z, ZHOU J, QIE L, HUANG Y H. Two-plateau Li-Se chemistry for high volumetric capacity Se cathodes[J]. Angew. Chem.-Int. Edit., 2020,59(33):13908-13914

[3]LIM J B, KIM H J, NA J H, KIM J K, JEONG S Y, PARK S K. Hierarchical nitrogen-doped multichannel carbon nanofibers for efficient potassium-selenium batteries[J]. Rare Met., 2025,44(6):3839-3851

[4]HUANG X L, WANG W, DENG J H, GAO W, LIU D Y, MA Q R, XU M W. A Se-hollow porous carbon composite for high-performance rechargeable K-Se batteries[J]. Inorg. Chem. Front., 2019,6(8):2118-2125

[5]ZHAO C H, LUO J S, HU Z B. Hierarchical porous N,O Co-doped carbon/Se composite derived from hydrothermal treated chitosan as Li-Se battery cathode[J]. Micro Nano Lett., 2018,13(10):1386-1389

[6]XIA M T, FU H W, LIN K R, RAO A M, CHA L M, LIU H, ZHOU J, WANG C X, LU B A. Hydrogen-bond regulation in organic/aqueous hybrid electrolyte for safe and high-voltage K-ion batteries[J]. Energ. Environ. Sci., 2024,17(3):1255-1265

[7]YE W K, LI W Y, WANG K, YIN W H, CHAI W W, QU Y, RUI Y C, TANG B H J. ZIF-67@Se@MnO_2: A novel Co-MOF-based composite cathode for lithium selenium batteries[J]. J. Phys. Chem. C, 2019,123(4):2048-2055

[8]SONG J P, WU L, DONG W D, LI C F, CHEN L H, DAI X, LI C, CHEN H, ZOU W, YU W B, HU Z Y, LIU J, WANG H E, LI Y, SU B L. MOF-derived nitrogen-doped core-shell hierarchical porous carbon confining selenium for advanced lithium-selenium batteries[J]. Nanoscale, 2019,11(14):6970-698

[9]JO D, LIM J B, KIM J K, KANG Y C, PARK S K. Three-dimensional carbon microclusters organized by hollow carbon nanospheres for stable Li metal anodes: Enabling high packing density and low tortuosity via self-assembly[J]. Rare Met., 2025,44(1):95-109

[10]ZHOU L, CUI Y P, KONG D Q, FENG W T, GAO X L, YAN Y G, REN H, HU H, XUE Q Z, YAN Z F, XING W. Amorphous Se species anchored into enclosed carbon skeleton bridged by chemical bonding toward advanced K-Se batteries[J]. J. Energy Chem., 2021,61:319-326

[11]CHENG L, MA C H, LU W Q, WANG X, YUE H J, ZHANG D, XING Z Y. A graphitized hierarchical porous carbon as an advanced cathode host for alkali metal-selenium batteries[J]. Chem. Eng. J., 2022,433:133527

[12]GUO B R, MI H W, ZHANG P X, REN X Z, LI Y L. Free-standing selenium impregnated carbonized leaf cathodes for high-performance sodium-selenium batteries[J]. Nanoscale Res. Lett., 2019,14:2861

[13]DING J N, WANG Y D, HUANG Z C, SONG W Q, ZHONG C, DING J, HU W B. Toward theoretical capacity and superhigh power density for potassium-selenium batteries via facilitating reversible potassiation kinetics[J]. ACS Appl. Mater. Interfaces, 2022, 14(5):6828-6840

[14]DENG W N, LI Y H, XU D F, ZHOU W, XIANG K X, CHEN H. Three-dimensional hierarchically porous nitrogen-doped carbon from water hyacinth as selenium host for high-performance lithium-selenium batteries[J]. Rare Met., 2022,41(10):3432-3445

[15]WANG H A, WANG P T, CAO J P, LIANG C, YU K F. N/S co-doped biomass-based porous carbon surface-embedded small-molecule selenium as cathode circumflex accent a for high-performance K-Se batteries[J]. Electrochim. Acta, 2022, 432(10):141158

[16]WU X Y, CHEN X, WU H Y, XIE B, WANG D G, WANG R, ZHANG X Y, PIAO Y Z, DIAO G W, CHEN M. Encapsulation of Se in dual-wall hollow carbon spheres: Physical confinement and chemisorption for superior Na-Se and K-Se batteries[J]. Carbon, 2022,187:354-364

[17]LYU W, YU X Z, LV Y W, RAO A M, ZHOU J, LU B G. Building stable solid-state potassium metal batteries[J]. Adv. Mater., 2024,36(24):2305795

[18]DONG W D, YU W B, XIA F J, CHEN L D, ZHANG Y J, TAN H G, WU L, HU Z Y, MOHAMED H S H, LIU J, DENG Z, LI Y, CHEN L H, SU B L. Melamine-based polymer networks enabled N, O, S Co-doped defect-rich hierarchically porous carbon nanobelts for stable and long-cycle Li-ion and Li-Se batteries[J]. J. Colloid Interface Sci., 2021,582:60-69

[19]XIA Q, HU J L, CHEN Q Q, ZHANG L Z. Highly N-doped and flexible carbon nanofiber membrane as cathode host for Li-Se batteries [J]. J. Alloy. Compd., 2022,927:167014

[20]GAO F, YUE X A, XU X Y, XU P, ZHANG F, FAN H S, WANG Z L, WU Y T, LIU X, ZHANG Y. A N/Co co-doped three-dimensional porous carbon as cathode host for advanced lithium-selenium batter-

ies[J]. Rare Met., 2023,42(8):2670-2678

[21]LIM J B, PARK S K. Novel N-doped multichannel carbon nanofiber architecture with porous CoS nanoprisms for high-performance potassium-ion batteries[J]. Rare Met., 2024,43(3):971-983

[22]LIM J B, NA J H, KIM H J, KIM J K, YOO Y, PARK S K. Electrospun MOF-derived N-doped mesoporous carbon fibers embedded with ultrafine vanadium oxide as an ultralong cycling stability for potassium ion storage[J]. J. Alloy. Compd., 2024,1002:175507

[23]KANG J Z, YU H, JING H B, HUANG L S, WANG J J, WANG X M, ZHAO X Y, QI W H, DU C F. Screening and activating small-molecule Se in microporous S-decorated/N-doped carbon spheres for an enhanced rate performance[J]. Appl. Surf. Sci., 2023,619:156724

[24]KIM J K, KANG Y C. Encapsulation of Se into hierarchically porous carbon microspheres with optimized pore structure for advanced Na-Se and K-Se batteries[J]. ACS Nano, 2020,14(10):13203-13216

[25]CHEN X, XU L H, ZENG L X, WANG Y Y, ZENG S H, LI H Z, LI X Y, QIAN Q R, WEI M D, CHEN Q H. Synthesis of the Se-HPCF composite via a liquid-solution route and its stable cycling performance in Li-Se batteries[J]. Dalton Trans., 2020,49(41):14536-14542

[26]ZHOU J, CHEN M X, WANG T, LI S Y, ZHANG Q S, ZHANG M, XU H J, LIU J L, LIANG J F, ZHU J, DUAN X F. Covalent selenium embedded in hierarchical carbon nanofibers for ultra-high areal capacity Li-Se batteries[J]. iScience, 2020,23(3):100919

[27]KALIMUTHU B, NALLATHAMBY K. Designed formulation of Se-impregnated N-containing hollow core mesoporous shell carbon spheres: Multifunctional potential cathode for Li-Se and Na-Se batteries[J]. ACS Appl. Mater. Interfaces, 2017,9(32):26756-26770

[28]ZHAO X S, YIN L C, ZHANG T, ZHANG M, FANG Z B, WANG C Z, WEI Y J, CHEN G, ZHANG D, SUN Z H, LI F. Heteroatoms dual-doped hierarchical porous carbon-selenium composite for durable Li-Se and Na-Se batteries[J]. Nano Energy, 2018,49:137-146

[29]LU S J, LIN J Y, WANG C H, ZHANG Y F, ZHANG Y, FAN H S. Heterogeneous engineering of MnSe@NC@ReS_2 core-shell nanowires for advanced sodium-/potassium-ion batteries[J]. Rare Met., 2024,43(8):3713-3723

[30]GAO X J, YANG X F, WANG S Z, SUN Q, ZHAO C T, LI X N, LIANG J W, ZHENG M, ZHAO Y, WANG J W, LI M S, LI R, SHAM T K, SUN X L. A 3D-printed ultra-high Se loading cathode for high energy density quasi-solid-state Li-Se batteries[J]. J. Mater. Chem. A, 2020,8(1):278-286

[31]DING J, ZHOU H, ZHANG H, STEPHENSON T, LI Z, KARPUZOV D, MITLIN D. Exceptional energy and new insight with a sodium-selenium battery based on a carbon nanosheet cathode and a pseudographite anode[J]. Energ. Environ. Sci., 2017,10(1):153-165

[32]ZHANG H, JIA D D, YANG Z W, YU F Q, SU Y L, WANG D J, SHEN Q. Alkaline lignin-derived porous carbon as an efficient scaffold for lithium-selenium battery cathode[J]. Carbon, 2017,122:547-555

[33]YUAN B B, SUN X Z, ZENG L C, YU Y, WANG Q S. A freestanding and long-life sodium-selenium cathode by encapsulation of selenium into microporous multichannel carbon nanofibers[J]. Small, 2018,14(9):1703252

[34]MUKKABLA R, DESHAGANI S, MEDURI P, DEEPA M, GHOSAL P. Selenium/graphite platelet nanofiber composite for durable Li-Se batteries[J]. ACS Energy Lett., 2017,2(6):1288-1295

[35]YI Z Q, YUAN L X, SUN D, LI Z, WU C, YANG W J, WEN Y W, SHAN B, HUANG Y H. High-performance lithium-selenium batteries promoted by heteroatom-doped microporous carbon[J]. J. Mater. Chem. A, 2015,3(6):3059-3065

[36]CAI Q F, LI Y Y, WANG L, LI Q W, XU J, GAO B, ZHANG X M, HUO K F, CHU P K. Freestanding hollow double-shell Se@CN_x nanobelts as large-capacity and high-rate cathodes for Li-Se batteries[J]. Nano Energy, 2017,32:1-9

[37]LI H X, LANG J W, LEI S L, CHEN J T, WANG K J, LIU L Y, ZHANG T Y, LIU W S, YAN X B. A high-performance sodium-ion hybrid capacitor constructed by metal-organic framework-derived anode and cathode materials[J]. Adv. Funct. Mater., 2018, 28(30): 1800757